IOPscience iopscience.iop.org

Home Search Collections Journals About Contact us My IOPscience

The structural evolution of InN nanorods to microstructures on Si (111) by molecular beam epitaxy

This content has been downloaded from IOPscience. Please scroll down to see the full text.

2014 Semicond. Sci. Technol. 29 085010

(http://iopscience.iop.org/0268-1242/29/8/085010)

View the table of contents for this issue, or go to the journal homepage for more

Download details:

IP Address: 148.88.190.107

This content was downloaded on 30/03/2015 at 11:16

Please note that terms and conditions apply.

OPEN ACCESS

Made open access 15 December 2014

IOP Publishing

Semiconductor Science and Technology

Semicond. Sci. Technol. **29** (2014) 085010 (7pp)

doi:10.1088/0268-1242/29/8/085010

The structural evolution of InN nanorods to microstructures on Si (111) by molecular beam epitaxy

E A Anyebe, Q Zhuang, M Kesaria and A Krier

Department of Physics, Lancaster University, Lancaster LA1 4YB, UK

E-mail: q.zhuang@lancaster.ac.uk

Received 23 March 2014, revised 12 May 2014
Accepted for publication 28 May 2014
Published 24 June 2014

Abstract

We report the catalyst free growth of wurtzite InN nanorods (NRs) and microislands on bare Si (111) by plasma-assisted molecular beam epitaxy at various temperatures. The morphological evolution from NRs to three dimensional (3D) islands as a function of growth temperature is investigated. A combination of tapered, non-tapered, and pyramidal InN NRs are observed at 490 °C, whereas the InN evolves to faceted microislands with an increase in growth temperature to 540 °C and further developed to indented and smooth hemispherical structures at extremely high temperatures (630 °C). The evolution from NRs to microislands with increase in growth temperature is attributed to the lowering of the surface free energy of the growing crystals with disproportionate growth velocities along different growth fronts. The preferential adsorption of In atoms on the (0001) c-plane and (10-10) m-plane promotes the growth of NRs at relatively low growth temperature and 3D microislands at higher temperatures. The growth rate imbalance along different planes facilitates the development of facets on 3D microislands. A strong correlation between the morphological and structural properties of the 3D films is established. XRD studies reveal that the NRs and the faceted microislands are crystalline, whereas the hemispherical microislands grown at extremely high growth temperature contain In adlayers. Finally, photoluminescent emissions were observed at ~0.75 eV from the InN NRs.

Keywords: InN, nanorods, nanostructures, structural evolution, molecular beam epitaxy, microstructures

(Some figures may appear in colour only in the online journal)

1. Introduction

Among group III nitride wide band-gap semiconductors, indium nitride (InN) has attracted attention due to its unique properties such as low effective mass, high carrier mobility, relatively high absorption coefficient and narrow band gap energy (0.7–0.9 eV) [1, 2]. Consequently, InN holds enormous potential in various device applications including lasers, high-speed field-effect transistors [3] and nanogenerators [4]. Despite this huge potential, the growth of InN has been very challenging due to its low decomposition temperature, the high equilibrium vapour pressure of nitrogen over indium and the shortage of lattice-matched substrates. Various substrates have been used for the growth of InN but Si substrate is the most attractive alternative owing to its low cost, large sizes (up to 12 inch diameter) and relatively small thermal mismatch [5]. Although crystalline InN films with dislocation density of ~10^8 cm^{-2} have been successfully grown by various techniques [6], the desire for single crystalline InN with significantly reduced dislocation density still persists. One-dimensional nanorods (NRs) materials have emerged as an alternative to their bulk counterparts. NRs have a number of advances including large surface-to-volume ratio, high density of electronic states, diameter-dependent band gap, enhanced optical absorption and dislocation-free structures on foreign substrates [7, 8]. However, there are challenges in the growth of catalyst free InN nanostructures such as the low dissociation temperature, high indium (In) migration rate and

© 2014 IOP Publishing Ltd Printed in the UK

Content from this work may be used under the terms of the Creative Commons Attribution 3.0 licence.
Any further distribution of this work must maintain attribution to the author(s) and the title of the work, journal citation and DOI.

Table 1. Growth parameters and morphologies of the investigated samples.

Sample	Growth Temp (°C)	Growth Time (hrs)	Morphology	Distinctive features
A	490	3.18	Nanorods	Untapered, Tapered and Pyramidal
B	520	0.87	Microislands	Lightly faceted (LF)
C	540	2.48	Microislands	Deeply faceted (DF)
D	560	3.02	Microislands	Indented hemispheres (IH)
E	630	4.23	Microislands	Smooth hemispheres (SH)

the tapered morphology resulting from the continuous formation of nucleation sites during simultaneous introduction of In and nitrogen species.

Given the enormous potential device applications of InN NRs, the narrow growth temperature window and specifically the requirement of higher growth temperature for InGaN to construct heterostructures, it is essentially important to investigate the growth and morphology of InN NRs at high temperatures. A previous study [9] has focused on the growth conditions for the evolution of InN NRs from compact layers on AlN buffered-Si (111) layers. It was found that nitrogen rich condition favours the formation of NRs, whereas stoichiometric conditions lead to coalescence of InN layers. The structural evolution from NRs to polycrystalline micro-grains on AlN buffered layer has been investigated [10]. Chang *et al* [3] have developed an In seed-assisted growth technique which led to uniform dislocation-free InN NRs with a record narrow PL spectral line width of 14 meV at 5 K, whereas the absence of In seeding layer resulted in morphologically inferior, severely tapered NRs which indicates that the In adatom diffusion on the surface plays a crucial role on the growth of NRs. The optimal NRs growth conditions and the influence of growth temperature (T_g) on the morphology of InN NRs within the 440–525 °C growth temperature regime has been previously identified [11]; non-uniform and shaped NRs were obtained with a rise in temperature to 525 °C. However, a detailed investigation of the morphology and crystal structure of NRs at high temperatures beyond 525 °C is still lacking. Furthermore, little is known about the maximum temperature at which NRs can be obtained along with the conditions for the evolution from NRs to microislands. In this study, we report the initial stages of InN NRs growth, the morphological evolution from NRs to microislands at high growth temperatures >490 °C, as well as the detailed properties, geometry and crystal structure.

2. Experimental details

The samples were grown on Si (111) substrates by plasma-assisted molecular beam epitaxy (VG-V80H MBE equipped with an oxford Applied Research HD25 radio-frequency nitrogen plasma source). The substrates were chemically cleaned using 10% hydrofluoric acid solution to remove the surface native oxide then immediately loaded into the MBE system to avoid re-oxidation. The substrates were then outgassed at 650 °C for >3 h. The nitrogen plasma power, N and In beam equivalent pressure (BEP) were set at 270 W, 7.0×10^{-5} and 2.3×10^{-7} mbar, respectively (N/In BEP ratio ≈300). A 5 nm 2D equivalent In layer was initially deposited, followed by the growth of InN film by simultaneously opening the shutters for In and nitrogen plasma. All the InN films were grown at similar N/In BEP ratio (≈300) but at different growth time and substrate temperatures (T_g) which were measured by a thermocouple. The surface morphology of the resulting samples was determined by a Sirion field-emission scanning electron microscope (FESEM). X-ray diffraction (XRD) was employed to investigate the crystalline quality. Photoluminescence (PL) measurements were used to investigate the optical properties of the 3-dimensional (3D) InN films in comparison to a 2D InN thin film reference sample using an Ar+ ion laser (514 nm) with an InSb detector.

3. Results and discussions

The growth parameters and the surface morphologies of the grown samples are summarised in table 1. The morphological evolution of the 3D InN films grown at T_g ranging from 490 to 630 °C is depicted in figures 1(a)–(e). The morphology of InN films exhibits 3D features varying from nanometre to micron size structures of various shapes ranging from columnar, lightly faceted to deeply faceted microislands, indented hemispheres and smooth hemispherical microislands.

Figure 1(a) shows the FESEM image of InN thin film grown at 490 °C which has protruding 3D NRs. Some of the NRs are *c*-axis oriented and non-tapered while others are tilted with respect to the substrate normal. The inset of 1(a) highlights the hexagonal NRs which are oriented normal to the substrate, non-tapered (NT) and aligned along the [0001] direction. A detailed examination of the NRs ($T_g = 490$ °C) reveal the initial stages of longer InN NRs reported in literature [12].

As highlighted in figure 2, the tilted NRs have different angles of inclination (denoted as θ_1 and θ_2 in the inset) with respect to the Si (111) substrate. Thus, on the basis of inclination they are categorized as left-tapered (LT), right-tapered (RT), fully-tapered (FT) and pyramidal (PM). The identified crystal planes of the NRs side faces correspond to hexagonal InN and are summarized in table 2.

The observed NRs morphologies could be associated with kinetic processes governing the initial InN NRs growth phase with the possibility of obtaining both tapered and non-tapered NRs as illustrated in figure 3. The sticking coefficient

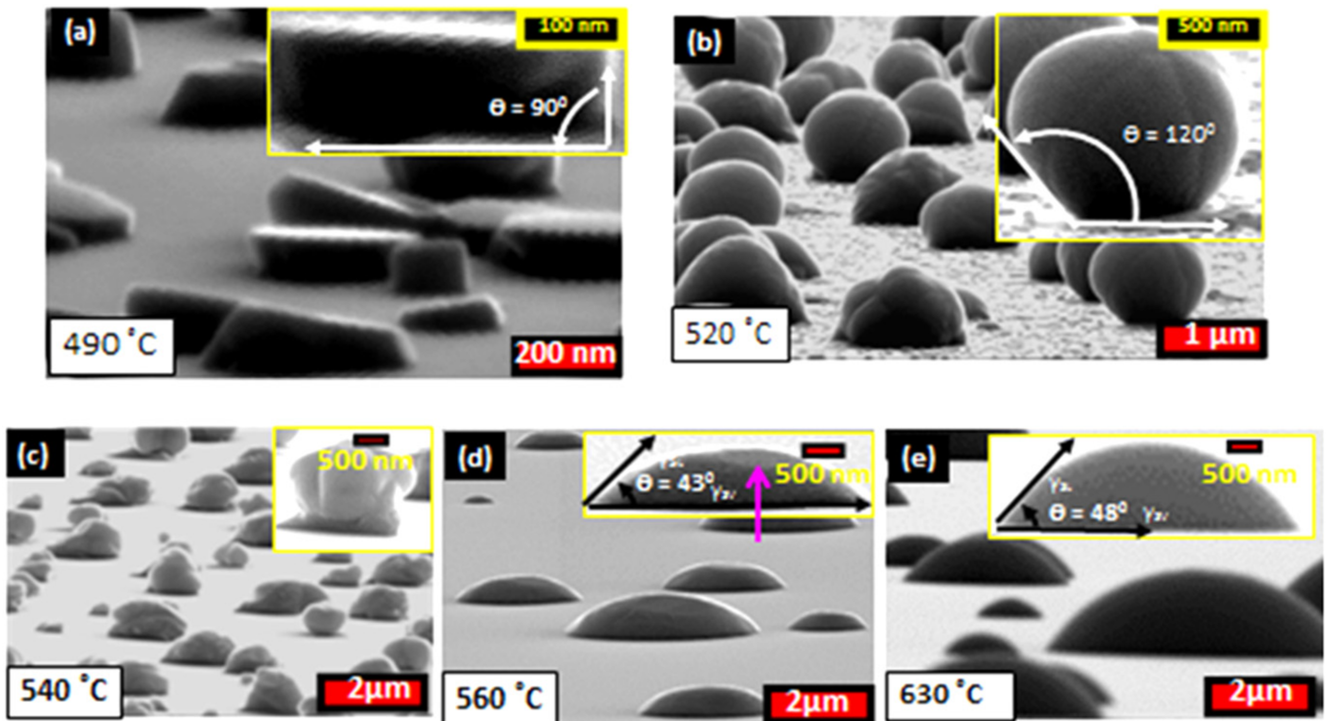

Figure 1. FESEM images of the surface morphology of typical InN NRs deposited at a temperature of 490 °C (a); and microislands grown at (b) 520 °C, (c) 540 °C, (d) 560 °C and (e) 630 °C. The insets show the high magnification images of the representative features.

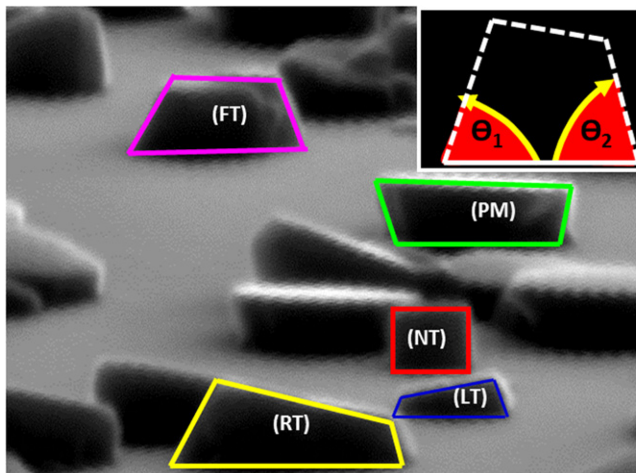

Figure 2. SEM micrograph showing the NRs structures with different orientations to the Si (111) substrate.

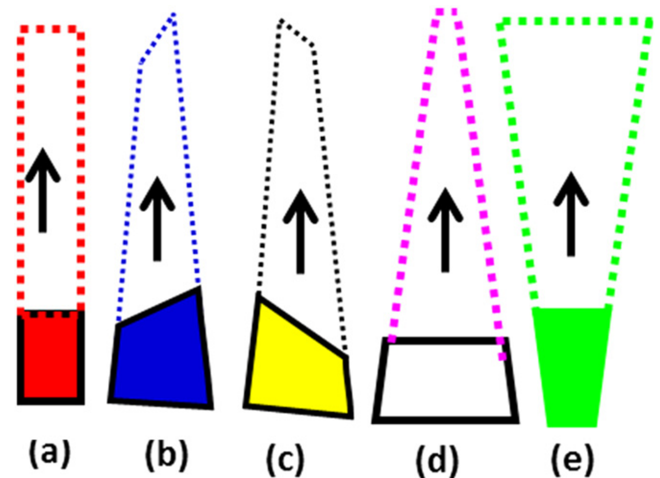

Figure 3. Schematic of possible morphologies of InN NRs.

of plane (0001) > (10-10) > (1-102) > (10-11) [13, 14], thus impinging In and N adatom are more favourable to grow on (0001) c-plane than the (10-10) m-plane.

The contribution to NRs formation will be from the direct impingement at the topmost surface, the adatoms diffusion along the sidewalls to the tip and diffusion from the substrate to NRs sidewalls. It is generally believed that the In adatom diffusion from the substrate to the NRs sidewall and from the sidewall to the tip is crucially important for the growth of non-tapered NRs, we speculate that the tapering and random alignment of the NRs relative to the substrate is associated with the non-uniform availability of In adatoms at the NRs base, sidewalls and tip during nucleation and the early stage of NRs growth. However, it should be noted that the observed morphological variation in our NRs compared to recent studies [15, 16] which also employed In droplets as seeds for the nucleation of highly symmetric NRs could be attributable to differences in growth conditions (higher In flux, lower plasma RF power and slightly higher T_g). A more detailed investigation of the observed trend is undoubtedly required to further confirm our speculation; however, that is beyond the scope of this report. Work is ongoing for the time dependent and low temperature InN NRs growth at temperatures ⩽490 °C.

The 3D InN films grown at temperature >490 °C exhibit microislands with various morphologies. The inset of

Table 2. Morphologies and crystal planes of InN Nanorods grown at 490 °C.

Typical NR	Morphology of NRs	Angle of inclination to Si (111) substrate (θ_1)(degrees)	Crystal plane	Angle of inclination to Si (111) substrate (θ_2)(degrees)	Crystal Plane
A	Non-tapered	90	(10–10)	90	(10–10)
B	Left-tapered	58	(30–34)	75	(20–21)
C	Right-tapered	58	(30–34)	75	(20–21)
D	Fully-tapered	61	(10–11)	61	(10–11)
E	Pyramidal	79	(30–31)	72	(50–53)

figure 1(b) shows the high magnification image of emerging lightly faceted (LF) microislands observed in InN film grown at 520 °C. It appears to be the commencement of faceted islands growth with less conspicuous cusp. These islands evolve into deeply faceted (DF) 3D island with more pronounced, distinct and outwardly bulging cusps as the growth temperature was increased to 540 °C (higher magnification image shown in the inset of figure 1(c)). The evolution of these DF islands can be explained using the Wulff construction [17] which is illustrated in figure 4.

It has been demonstrated that wurtzite InN microstructures grow along the [0001] direction under high N/III flux while low N/III flux leads to growth along <10-10> directions [18].

Although a high N/III flux ratio was initially supplied during growth, the high growth temperature increases InN desorption leading to an indium rich condition, which results in a preferential adsorption of In atoms. Consequently, the <10-10> direction possesses the lower surface energy in comparison to the [0001]. The slower growth rate along the m-direction <1-100> leads to concave facets and relative faster growth along a-direction <11-20> thereby tending toward convex facets. This imbalance in growth rate along m and a-directions creates six cusps along the closed curve, which can be observed if the cross-section of these microstructures can be seen. These exterior facets are distinctive of the early stage of island development. With an increase in T_g to 560 °C, the microislands morphology transforms to indented hemispherical (IH) structures (as shown in the inset of figure 1(d)) with a typical contact angle of 43° and shallow pits (as denoted by the pink arrow) which disappear as T_g is further increased to 630 °C. Extremely high growth temperature leads to the formation of spherical hemispherical (SH) islands with a contact angle of 48°. These SH are very smooth and hemispherical in shape (figure 1(e)). Both IH and SH microislands are morphologically different to the LF and DF samples with no observable facets.

In addition, it is likely that growth kinetics play a crucial role in the observed shape transformations. Driven by the anisotropy of surface energies coupled with the scaling growth anisotropy, the morphology of the nanostructures is modified as the structures grow [19], typical of self-assisted NRs growth.

The unique features of the IH and SH microislands prompted the investigation of these films by XRD and optical microscopy in order to understand the formation of the InN films. Figure 5 shows the XRD pattern of InN NRs at 490 °C

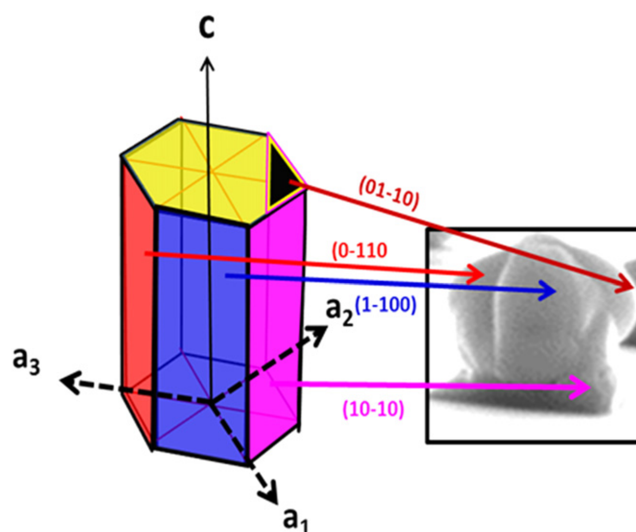

Figure 4. Schematic of hexagonal lattice showing c-plane and m-plane InN surfaces.

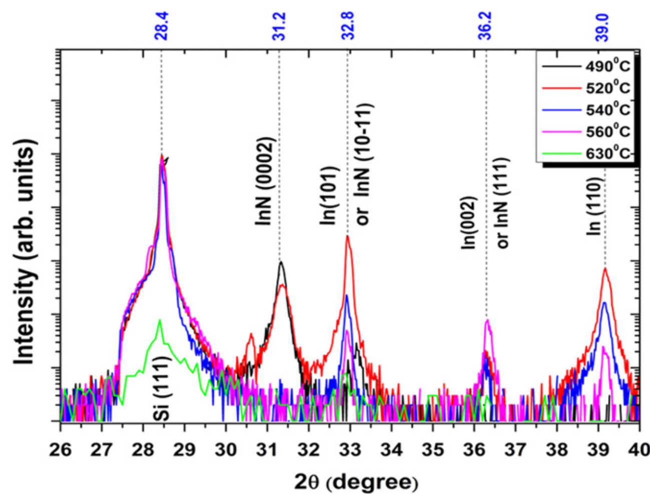

Figure 5. X-ray diffraction patterns of InN nanorods and microislands grown at 490 °C and (520 °C–630 °C) respectively.

and microislands at (520–630 °C), respectively. The relative intensities of the diffraction peaks are plotted against the growth temperature (figure 6) to identify the dominant diffraction peak and crystal orientations of the grown samples. Shown in the inset of figure 6 is the schematic of the (0002) and (10-11) InN crystal planes for the observed reflections from samples. Analysis of the XRD result suggests the InN NRs formed at 490 °C are single-crystalline and wurtzite,

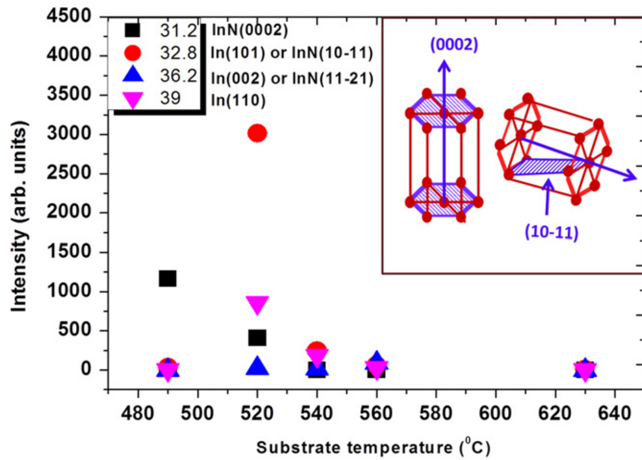

Figure 6. Plot of x-ray diffraction peak intensities of InN nanostructures as a function of growth temperature. The inset is the schematic of the (0002) and (10–11) InN crystal planes.

aligned along the [0001]. The presence of the reflection from (10-11) s-plane is due to the preferential growth of some nanocrystals along with s-direction [10-11] normal to the substrate.

The InN microislands grown at 520 °C exhibit similar preferences, moreover, there are other reflections present suggesting formations of In adlayer on the surface between the microislands. Although the InN microislands deposited at 540 °C are single-crystalline and wurtzite, the presence of strong (10-11) reflection suggests the microislands grew with (10-11) s-plane parallel to substrate or the single-crystalline In adlayer grown alongside. On indexing XRD patterns of films grown at 560 °C and 630 °C, it is clear that none of the reflections matches that of wurtzite InN which suggests no formation of wurtzite InN; instead In adlayer was deposited. Under optical microscope the sample grown at 490 °C has a dark surface. Whereas the 520 °C and 540 °C samples have a grey appearance, samples grown at 560 °C and 630 °C are shiny. Based on these investigations, we can conclude that no In adlayer is present on the surface of the single-crystalline InN NRs sample grown at 490 °C. Although the InN micrograins samples grown at 520 °C and 540 °C are both single-crystalline aligned along [0001] and [10-11] directions, respectively; both have the presence of In adlayer on the sample surface grown alongside the InN. The appearance of films grown at 560–630 °C suggests the possibility of amorphous InN or In film [20]. However, we cannot exclude the presence of In seeds, especially during NRs growth at a lower T_g [21].

The residual strain in the film is estimated to correlate the observed morphology of the InN films. The symmetric InN (0002) peak was observed at 2θ values of 31.33° and 31.37° for films grown at 490 °C and 520 °C, respectively, corresponding to the off-axis (10-11) s-plane whose 2θ values were identified at 33.15° and 33.30°, respectively. The InN lattice parameters were computed from the identified 2θ InN (0002) and (10-11) plane values. Similarly, the lattice parameters of the tetragonal In adlayers were deduced from the observed In (002) and (101) peaks. Both a-plane (ε_{xx}) and c- plane (ε_{zz}) strain values were then calculated using:

$$\varepsilon_{xx} = \frac{a - a_0}{a_0}$$
$$\varepsilon_{zz} = \frac{c - c_0}{c_0} \quad (1)$$

Where a and c are the calculated lattice parameters of the films and a_0 and c_0 are the lattice parameters of the bulk.

The c-plane stress (σ) was computed using Hooks law:

$$\sigma = \frac{[c - c_0]}{c_0}\frac{E}{\upsilon} \quad (2)$$

where c is the lattice parameter of the nanostructures, c_0 is the lattice parameter of the bulk, E is the bulk modulus (139 Gpa for InN and 42.2 Gpa for In) and υ is the poisson ratio (0.21 for InN and 0.45 for In).

The calculated lattice parameters, strain and stress values obtained for the films obtained from the XRD measurement are shown in table 3.

The NRs (490 °C) are fully relaxed along the c-plane with its lattice parameter matching that of bulk InN (5.703 Å) but under a thermally induced uniaxial in-plane compressive strain resulting from differences in in-plane lattice parameters of the Si(111) and the NRs. Compressive biaxial stress was imposed on the sample grown at 520 °C probably due to the large lattice mismatch (7.6%) between InN and Si (111) which can be fully or partially relieved through the creation of misfit dislocations at the interface between the epilayer and the substrate [22]. From the tetragonal In lattice parameters it is observed that biaxial tensile stress was present in the InN nanoislands grown at 520 °C and 540 °C which could be attributed to the gradual creation of misfit dislocations at the edges of the islands during their growth [23]. The observation of biaxial tensile stress has been associated with 3D growth mode [22]. This further corroborates our XRD results. A remarkable dependence of the sign of the strain on the shape and crystal is observed as the in-plane tensile strain is changed to compressive strain accompanying a morphological transition from faceted InN microislands to hemispherical In microislands. A gradual increase in the stress values is clearly seen with the morphological evolution from NRs to faceted InN Islands and finally In hemispheres. A salient feature explicated from table 3 is a close correlation between the C_{13}/C_{33} values and the nanostructures; all the InN films have negative C_{13}/C_{33} values as against the positive C_{13}/C_{33} values obtained for the In Islands.

Low temperature PL investigation of the NRs was carried out; the 4 K PL spectra compared to a 2D thin film are shown in figure 7. Bright emissions at ~0.75 eV are clearly visible from the NRs consistent with a previous report [24]. The observed blue-shift can be associated to the Burstein–Moss [25] shift resulting from the very large surface-to-volume ratios of the NRs. The observable low energy shoulder is attributed to the Urbach tail populated by the transition of degenerate electrons to the shallow acceptor states [26, 27].

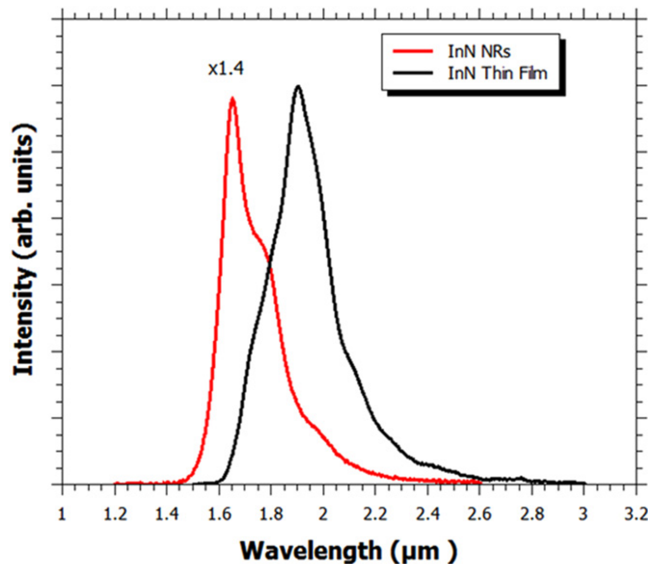

Figure 7. 4 K PL spectra of InN Nanorods compared with InN thin film.

Finally, the NRs have a narrower full width at half maximum (FWHM) of 50 meV as against 105 meV for the thin film.

4. Conclusions

The morphological evolution of 3D InN films is reported. We tried to understand in this study the cause for the observed morphological changes with increasing growth temperature. Governed by Wulff construction [17] the quest to lower the surface free energy of growing crystal has been identified as the primary motivation for the observed morphological transformations. The relative growth velocities along different growth fronts are dictated by the stoichiometry of precursors and by implication the growth temperature. The imposition of a kinetic energy barrier, suppression of In adatoms surface migration and subsequent reduction in adatom diffusion length coupled with the preference for axial growth with increasing N/III flux [28, 29] ratio favours a reduction in lateral growth and the evolution of NRs at $T_g = 490\,°C$. Conversely, high growth temperature ($T_g \geqslant 520\,°C$) increases the In adatom's kinetic energy, mobility and diffusion length [30] leading to a significant increase in lateral growth and the eventual emergence of microislands [31].

References

[1] Davydov V Y *et al* 2002 *Phys. Status Solidi* B **230** R4
[2] Davydov V Y *et al* 2002 *Phys. Status Solidi* B **229** R1
[3] Chang Y-l, Li F, Fatehi A and Mi Z 2009 *Nanotechnology* **20** 345203
[4] Ku N-J, Wang C-H, Huang J-H, Fang H-C, Huang P-C and Liu C-P 2013 *Adv. Mater.* **25** 861
[5] Grandal J, Sánchez-García M A, Calleja E, Luna E and Trampert A 2007 *Appl. Phys. Lett.* **91** 021902
[6] Liang W, Tsen K T, Ferry D K, Hai L and William J S 2004 *Appl. Phys. Lett.* **84** 3681
[7] Tchernycheva M *et al* 2007 *Nanotechnology* **18** 385306
[8] Hochbaum A I and Yang P 2010 *Chem. Rev.* **110** 527
[9] Calleja E *et al* 2007 *Phys. Phys. Status Solidi* B **244** 2816
[10] Hsiao C L, Tu L W, Chen M, Jiang Z W, Fan N W, Tu Y J and Wang K R 2005 *Jpn. J. Appl. Phys. Physics* **44** L1076
[11] Stoica T, Meijers R, Calarco R, Richter T and Lüth H 2006 *J. Cryst. Growth* **290** 241
[12] Sánchez-García M A, Grandal J, Calleja E, Lazic S, Calleja J M and Trampert A 2006 *Phys. Status Solidi* B **243** 1490
[13] Kamimura J, Kishino K and Kikuchi A 2011 *Aip Advances* **1** 042145
[14] Kawaji M, Baba S and Kinbara A 1979 *Appl. Phys. Lett.* **34** 748
[15] Zhao S, Fathololoumi S, Bevan K H, Liu D P, Kibria M G, Li Q, Wang G T, Guo H and Mi Z 2012 *Nano Lett.* 2012 **12** 2877
[16] Zhao S, Le B H, Liu D P, Liu X D, Kibria M G, Szkopek T, Guo H and Mi Z 2013 *Nano Lett.* **13** 5509
[17] Leung B, Sun Q, Yerino C D, Han J and Coltrin M E 2012 *Semicond. Sci. Technol.* **27** 024005
[18] Liu H, Shi L, Geng X, Su R, Cheng G and Xie S 2010 *Nanotechnology* **21** 245601
[19] Dubrovskii V G, Consonni V, Trampert A, Geelhaar L and Riechert H 2012 *Phys. Rev. B: Condens. Matter* **85** 165317
[20] ElAhl A M S *et al* 2003 *J. Appl. Phys.* **94** 7749
[21] Mandl B, Stangl J, Hilner E, Zakharov A A, Hillerich K, Dey A W, Samuelson L, Bauer G, Deppert K and Mikkelsen A 2010 *Nano Lett.* **10** 4443
[22] Dimakis E, Iliopoulos E, Tsagaraki K, Adikimenakis A and Georgakilas A 2006 *Appl. Phys. Lett.* **88** 191918
[23] Matthews J W 1975 *Epitaxial Growth* ed J W Matt (New York: Academic) p 1335
[24] Kumar M, Bhat T N, Rajpalke M K, Roul B, Kalghatgi A T and Krupanidhi S B 2011 *Nanoscale Res. Lett.* **6** 609
[25] Wu J *et al* 2004 *Appl. Phys. Lett.* **84** 2805
[26] Klochikhin A, Davydov V, Emtsev V, Sakharov A, Kapitonov V, Andreev B, Lu H and Schaff W J 2006 *Phys. Status Solidi* A **203** 50

Table 3. The lattice parameters, stress and strain values calculated from the XRD data for the NRs and microislands.

Growth Temperature (°C)	N/III Flux Ratio	Morphology	XRD Diffraction peaks	Lattice Parameter 'a' (Å)	Lattice Parameter 'c' (Å)	Strain 'a' direction	Strain 'c' direction	Stress 'c' (Gpa)	Calculated C_{13}/C_{33}
490	304	Nanorods	InN	3.5377	5.7030	-2.06×10^{-3}	—	—	—
520	304	Microisland	InN	3.5190	5.6960	-7.33×10^{-3}	-1.23×10^{-3}	−0.812	−0.084
520	304	Microisland	In Adlayer	3.2523	4.9476	9.23×10^{-5}	3.23×10^{-4}	0.030	−1.750
540	304	Microisland	In Adlayer	3.2525	4.9502	1.54×10^{-4}	8.49×10^{-4}	0.080	−2.756
560	304	Microisland	In Adlayer	3.2512	4.9554	-2.46×10^{-4}	1.90×10^{-3}	0.178	3.862
630	302	Microisland	In Adlayer	3.2477	4.9698	-1.32×10^{-3}	4.81×10^{-3}	0.451	1.822

[27] Klochikhin A A, Davydov V Y, Emtsev V V, Sakharov A V, Kapitonov V A, Andreev B A, Lu H and Schaff W J 2005 *Phys. Rev.* B **71** 195207
[28] Norman D P, Tu L W, Chiang S Y, Tseng P H, Wadekar P, Hamad S and Seo H W 2011 *J. Appl. Phys.* **109** 063517
[29] Wang X, Che S-B, Ishitani Y and Yoshikawa A 2006 *Phys. Status Solidi* C **3** 1561
[30] Wang H, Jiang D S, Zhu J J, Zhao D G, Liu Z S, Wang Y T, Zhang S M and Yang H 2009 *J. Phys. D: Appl. Phys.* **42** 145410
[31] Johansson J, Svensson C P T, Mårtensson T, Samuelson L and Seifert W 2005 *J. Phys. Chem.* B **109** 13567